

Magnitude and timing of major white matter tract maturation from infancy through adolescence with NODDI

Kirsten M. Lynch^{a,*}, Ryan P. Cabeen^a, Arthur W. Toga^a, Kristi A. Clark^b

^a Laboratory of Neuro Imaging (LONI), USC Stevens Neuroimaging and Informatics Institute, Keck School of Medicine, University of Southern California, Los Angeles, CA, USA

^b Department of Neurology, Keck School of Medicine, University of Southern California, Los Angeles, CA, USA

ARTICLE INFO

Keywords:

Brain development
White matter
NODDI
Maturation
Diffusion MRI
Microstructure

ABSTRACT

White matter maturation is a nonlinear and heterogeneous phenomenon characterized by axonal packing, increased axon caliber, and a prolonged period of myelination. While current *in vivo* diffusion MRI (dMRI) methods, like diffusion tensor imaging (DTI), have successfully characterized the gross structure of major white matter tracts, these measures lack the specificity required to unravel the distinct processes that contribute to microstructural development. Neurite orientation dispersion and density imaging (NODDI) is a dMRI approach that probes tissue compartments and provides biologically meaningful measures that quantify neurite density index (NDI) and orientation dispersion index (ODI). The purpose of this study was to characterize the magnitude and timing of major white matter tract maturation with NODDI from infancy through adolescence in a cross-sectional cohort of 104 subjects (0.6–18.8 years). To probe the regional nature of white matter development, we use an along-tract approach that partitions tracts to enable more fine-grained analysis. Major white matter tracts showed exponential age-related changes in NDI with distinct maturational patterns. Overall, analyses revealed callosal fibers developed before association fibers. Our along-tract analyses elucidate spatially varying patterns of maturation with NDI that are distinct from those obtained with DTI. ODI was not significantly associated with age in the majority of tracts. Our results support the conclusion that white matter tract maturation is heterochronous process and, furthermore, we demonstrate regional variability in the developmental timing within major white matter tracts. Together, these results help to disentangle the distinct processes that contribute to and more specifically define the time course of white matter maturation.

1. Introduction

Human postnatal brain development is a complex process that follows a dynamic and temporally overlapping series of cellular events that includes the development and formation of axonal pathways through cellular proliferation, differentiation, synaptogenesis, apoptosis, and a prolonged period of myelination (Rice and Barone, 2000). Structural MRI enables the quantification of gross anatomical changes during development that reflect these cellular processes. Childhood and adolescence are marked by significant decreases in cortical gray matter, indicative of synaptic pruning (Gogtay et al., 2004; Huttenlocher, 1979), and increases in cerebral white matter, believed to reflect myelination (Matsuzawa et al., 2001; Miller et al., 2012).

Quantification of white matter microstructure *in vivo* is made possible

with diffusion MRI (dMRI), a technique that elucidates the underlying white matter organization by measuring water displacement patterns in the brain (Beaulieu, 2002). Diffusion tensor imaging (DTI) techniques have been used to probe microstructural changes in major white matter tracts. Developmental studies in children and adolescents using DTI have consistently demonstrated heterogeneous and nonlinear increases in fractional anisotropy (FA) with age (Clayden et al., 2012; Eluvathingal et al., 2007; Imperati et al., 2011; Krogsrud et al., 2016; Lebel et al., 2012, 2010; 2008; Lebel and Beaulieu, 2011; Tamnes et al., 2010; Ullman and Klingberg, 2016; Wierenga et al., 2015). While DTI-based metrics are sensitive to age-related changes in microstructure, they are not specific (Beaulieu, 2009; Pierpaoli and Basser, 1996). For example, an increase in FA may be due to an increase in neurite density, a decrease in orientation dispersion, or a combination of factors (Jones et al., 2013). Additionally,

* Corresponding author. Mark and Mary Stevens Neuroimaging and Informatics Institute, Laboratory of Neuro Imaging, Keck School of Medicine of USC, 2025 Zonal Ave, Office 204, Los Angeles, CA, 90033, USA.

E-mail address: kirsten.lynch@loni.usc.edu (K.M. Lynch).

<https://doi.org/10.1016/j.neuroimage.2020.116672>

Received 14 October 2019; Received in revised form 19 January 2020; Accepted 18 February 2020

Available online 21 February 2020

1053-8119/© 2020 The Authors. Published by Elsevier Inc. This is an open access article under the CC BY-NC-ND license (<http://creativecommons.org/licenses/by-nc-nd/4.0/>).

DTI measures suffer from partial volume effects due to free-water contamination and complex fiber orientations, which bias the diffusion-weighted signal and complicate the interpretation of changes in DTI parameters (Jones and Cercignani, 2010).

Multi-compartment dMRI models overcome these limitations by acquiring diffusion-weighted images at multiple gradient strengths in order to probe tissue compartments with different diffusion profiles (Assaf and Cohen, 2000; Stanisz et al., 1997). Neurite Orientation Dispersion and Density Imaging (NODDI) is a multi-compartment model that estimates tissue compartment parameters associated with free, hindered, and restricted diffusion (Zhang et al., 2012). NODDI models the intracellular volume fraction, known as neurite density index (NDI), and orientation dispersion index (ODI), which provide biologically meaningful measures that quantify specific microstructural processes. NDI measures the amount of restricted diffusion within a voxel and is considered an index of neurite density. ODI describes the degree of neurite angular variation, which allows for modeling the full spectrum of neurite orientation patterns observed in the brain.

Previous studies of white matter development using NODDI demonstrate age-related increases in NDI across tracts in childhood and adolescence (Chang et al., 2015; Geeraert et al., 2019; Jelescu et al., 2014; Kodiweera et al., 2015; Mah et al., 2017) and NDI has been shown to account for more age-related variance than DTI measures in development (Genc et al., 2017; Mah et al., 2017). In contrast, previous studies have shown that ODI remains relatively stable throughout late childhood and adolescence (Chang et al., 2015; Mah et al., 2017), however few studies have explored the trajectory of ODI from infancy through adolescence. These findings suggest that NODDI parameters are sensitive to unique developmental features in white matter and can provide complementary information to that provided with DTI.

The main limitation of calculating a global measure to characterize an entire white matter tract is that it may obscure potentially valuable information about focal developmental changes within the tract. Along-tract approaches provide a framework to ameliorate this limitation by characterizing the spatial pattern of diffusion parameters within individual white matter bundles. This tract-based approach also provides enhanced sensitivity to regional developmental trajectories in major white matter tracts. Previous diffusion studies using along-tract approaches found diffusion parameters and their developmental trajectories vary along the length of individual fiber bundles in toddlers (Goodlett et al., 2009; Johnson et al., 2014) and children/adolescents (Chen et al., 2016; Colby et al., 2011; Yeatman et al., 2012b). Therefore, it is reasonable to expect that NODDI measures will also demonstrate distinct regional patterns of development within white matter tracts but with the added benefit of providing enhanced sensitivity to microstructural features. Characterization of these diffusion features together with the DTI parameters FA, mean diffusivity (MD) and radial diffusivity (RD) will provide a more comprehensive understanding of microstructural processes in white matter during critical periods of brain maturation. Here, we propose to characterize the magnitude and timing of development reflected with NODDI parameters in major white matter tracts using an along-tract approach put forth by Colby et al. (2012). This approach first consistently parameterizes streamlines representing each bundle to match to a reference bundle; then the bundle is partitioned cross-sectionally into equidistant points that can be statistically analyzed across the population. In contrast to whole bundle analysis, this can provide enhanced sensitivity for the detection of heterochronous patterns of white matter development that may occur at finer anatomical scales than otherwise available when examining parameters averaged across entire bundles.

While some studies have explored the age-related NODDI parameter changes of major white matter tracts in infancy (Jelescu et al., 2014; Kunz et al., 2014) and childhood/adolescence (Chang et al., 2015; Geeraert et al., 2019; Genc et al., 2017; Mah et al., 2017), the present study is the first to examine the complete developmental trajectory through infancy, childhood, and adolescence. The purpose of this study

was to characterize the magnitude and timing of major white matter tract maturation with NODDI in a cross-sectional cohort of 104 participants (0.6–18.8 years). Furthermore, we utilize along-tract analyses to spatially characterize developmental patterns along the length of major white matter tracts. The NODDI microstructural parameters may provide unique insight into the complex development of white matter tracts during this dynamic period.

2. Materials and methods

2.1. Subjects

Neuroimaging and demographic data were obtained through the publicly accessible Cincinnati MR Imaging of NeuroDevelopment (C-MIND) data repository (<http://research.cchmc.org/c-mind>) at Cincinnati Children's Hospital (Holland et al., 2015). Participants had no self-reported history of head trauma or neurological, developmental or psychiatric disease. In total, 104 right-handed typically developing infants, children and adolescents between the ages of 0.6 and 18.8 years were included in the cross-sectional study ($M = 7.9$, $SD = 4.9$ years; 56 female). There were no significant sex differences in the age distribution of the cohort, $t(102) = 1.75$, $p = .09$. Parent/guardian consent were obtained for all subjects and procedures were approved by the Institutional Review Board of the Cincinnati Children's Hospital Medical Center (CCHMC).

2.2. Image acquisition

Participants and their families were provided with audio recordings and headphones to acclimatize children to the MRI environment prior to the day of scan using the desensitization procedure outlined in (Vannest et al., 2014). DWI data was acquired over two sessions to prevent younger children from becoming restless and compromising image quality due to motion. For infants and toddlers, scans were scheduled at night and acquired during non-sedated sleep. For older children, scans were acquired during the day when they were awake. MRI data was obtained at CCHMC using a Philips 3T Achieva system and a 32-channel head coil. Diffusion-weighted images (DWI) were obtained using a spin-echo, echo-planar imaging (EPI) method with intravoxel incoherent motion (IVIM) gradients. For each subject, 2 DWIs were obtained with the following parameters: 2 mm isotropic voxels, 112x109 acquisition matrix, and 61 noncollinear diffusion sensitizing gradient directions with 7 non-diffusion-weighted (b_0) images interspersed throughout the acquisition and averaged into a single image. The scans differed in the following parameters: (1) $TR = 6614$ ms, $TE = 81$ ms, $b = 1000$ s/mm² and (2) $TR = 8112$ ms, $TE = 81$ ms, $b = 3000$ s/mm². T1-weighted images were acquired for anatomical alignment using turbo-field echo MPRAGE sequence with the following parameters: 1 mm isotropic voxels, 256x224 × 160 mm FOV, $TI = 939$ ms, $TR = 8.1$ ms, $TE = 3.7$ ms.

2.3. Data preprocessing

C-MIND performed manual and automated quality control and co-registration prior to release. Quality assurance procedures adapted from the American College of Radiology (ACR) were employed (ACR, 2004). First, all $b = 0$ vol were loaded into a movie loop to identify overt processing failures. Next, the entire DWI dataset was run through DTI-Prep (<http://www.nitrc.org/projects/dtiprep>) to automatically detect signal drop out, slice interlace artifacts and excessive motion and volumes acquired with a given diffusion direction were discarded if they failed to meet the specified quality thresholds (Yuan et al., 2009). Last, each image was reviewed by a trained radiologist to identify disqualifying pathological abnormalities or anatomical distortions (Kaiser et al., 2015). For the present study, DWI shells with at least 45 diffusion directions were considered for analyses (Supplementary Table 1).

Images from each shell were separately preprocessed using FSL

(FMRIB, Oxford, UK), including corrections for motion and eddy current distortions using the `eddy_correct` module (Smith et al., 2004). All MRI images were then skull-stripped using FSL's BET (Smith, 2002). The NODDI model was estimated using multi-shell diffusion data acquired with different acquisition parameters, which may lead to model estimation errors. We mitigated the effects of unmatched diffusion protocols by normalizing the shells with the B0 volumes, as recommended in previous retrospective studies (Genc et al., 2018, 2017; Claire E. Kelly et al., 2016; Owen et al., 2014) and according to the developer's recommendation (Counsell et al., 2014). Signal normalization was performed by first producing a pair of average baseline scans from b0 images with matching TR and TE, then each diffusion weighted image was matched and normalized to its corresponding average baseline. Our implementation of the normalization procedure is available in the `VolumeDwiNormalize` module in QIT (<https://cabeen.io/qitwiki>). In order to perform multi-shell modeling with NODDI, the two DWIs per subject were co-registered to a common space with corrected gradient tables using AIR (Woods et al., 1998). For each subject, T1-weighted images were registered to the aligned DWI using an affine transformation with FSL's FLIRT (Jenkinson et al., 2002).

2.4. Microstructure parameters

NODDI and DTI parameters were calculated per voxel across each participant's brain in native space. DTI parameters were also included for template registration.

DTI Fractional anisotropy (FA), axial diffusivity (AD), radial diffusivity (RD) and mean diffusivity (MD) were computed using a two-stage weighted-least squares estimation scheme (Veraart et al., 2013). Quantification of developmental processes were carried out with FA, MD and RD.

NODDI NODDI parameters were estimated using in-house software based on the NODDI Matlab Toolbox (Zhang et al., 2012). The NODDI framework models 3 separate compartments: (1) the intracellular compartment, such as axons and dendrites, is modeled as zero-radius cylinders, (2) the extracellular compartment, such as glia and cell bodies, is modeled with Gaussian anisotropic diffusion, and (3) the cerebrospinal fluid (CSF) compartment is modeled with isotropic diffusion. The full normalized signal is a mixture of these 3 diffusion environments:

$$S = (1 - v_{iso})(v_{ic}S_{ic} + (1 - v_{ic})S_{ec}) + v_{iso}S_{iso} \quad (1)$$

where S is the full normalized signal; S_{ic} , S_{ec} , and S_{iso} are the normalized signals of the intracellular, extracellular, and CSF compartments, respectively; and v_{ic} and v_{iso} are the normalized tissue density estimates of the intracellular and CSF compartments, respectively (Zhang et al., 2012). The orientation dispersion index (ODI), which describes the extent that the FOD deviates from its primary diffusion direction, was modeled using the Watson distribution (Zhang et al., 2011a).

2.5. Fiber tracking

An atlas-based streamline tractography approach was used to obtain fiber bundle models from the DWI data using the Quantitative Imaging Toolkit (QIT) (Cabeen et al., 2018) and other software, noted where applicable. We first manually delineated reference fiber bundles in the IIT ICBM diffusion MRI template (Varentsova et al., 2014; Zhang et al., 2011b) using deterministic streaming tractography with a kernel regression framework (Cabeen et al., 2016). These reference bundles were segmented according to *a priori* anatomical information from white matter atlases and reference texts (Catani et al., 2002; Catani and de Schotten, 2012; Wakana et al., 2007), and resulted in seed, inclusion, and exclusion region of interest (ROI) masks for each tract. The diffusion tensor imaging data of each subject was used to compute a deformation from the template to subject space using the tensor-based deformable registration algorithm in DTI-TK (Zhang et al., 2006). The ROI masks for

each tract were transformed to subject native space for use in subject-specific bundle reconstruction. We used the tractography module `VolumeModelTracksStreamline` in QIT to extract bundle models using the ball-and-sticks models and bundles mask. The ball-and-sticks model was estimated using FSL `bedpostx` (Behrens et al., 2007), which is a Bayesian approach that estimates the number of diffusion compartments and accounts for isotropic diffusion, partial voluming and crossing fibers. We then reconstructed each bundle using the deterministic streamline tractography with model-based Trilinear interpolation (Cabeen et al., 2016) with an angle threshold of 75°, a step size of 0.5 mm, a minimum length of 10 mm, and Runge-Kutta integration. We used a minimum volume fraction of 0.05 which produced robust and comparable reconstructions of fiber bundles across the subject age range. For each bundle, seeding was initiated from 5 randomly placed samples within the deformed seed ROI mask, tracks were retained using the deformed inclusion and exclusion ROI masks, and a track density map was computed. The following 9 major bilateral major white matter tracts were reconstructed for analysis: forceps major (FMAJ), forceps minor (FMIN), anterior thalamic radiation (ATR), cingulum (CGC), corticospinal tract (CST), inferior fronto-occipital fasciculus (IFO), inferior longitudinal fasciculus (ILF), superior longitudinal fasciculus (SLF), and uncinate fasciculus (UNC) (Fig. 1). To address possible performance issues related to age-related differences in brain morphometry and image contrast, we performed comprehensive quality control of our results, in which all tracts were visually inspected and edited for anatomical accuracy in native space.

2.6. Along-tract processing

To enable more fine-grained analysis of NODDI and DTI parameters within white matter tracts, we employed an along-tract technique based on (Colby et al., 2012). This approach partitions each tract cross-sectionally into equidistant points using an automated process, described as follows. First, for each bundle in the template, a single

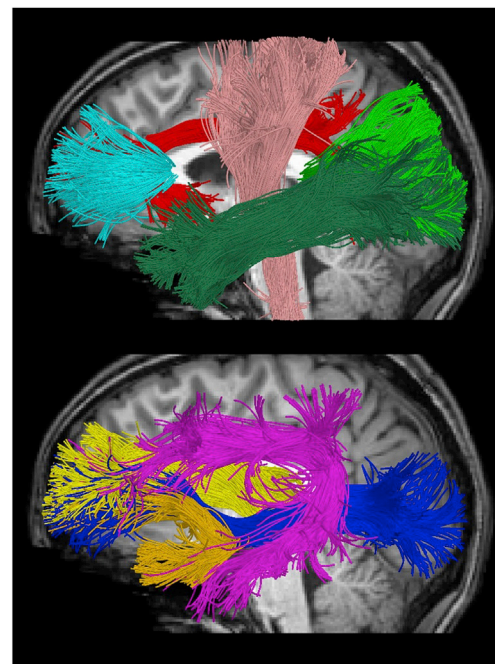


Fig. 1. Major white matter tracts used in the present study visualized using tractography in a sample subject.

(Top) forceps minor (FMIN), cingulum (CGC), corticospinal tract (CST), inferior longitudinal fasciculus (ILF) and forceps major (FMAJ). (Bottom) Anterior thalamic radiation (ATR), uncinate fasciculus (UNC), superior longitudinal fasciculus (SLF), inferior fronto-occipital fasciculus (IFO).

prototypical curve was found by identifying the “centroid” curve with the minimum Hausdorff distance to the others, and the curve was resampled with points every 5 mm to represent regions along the length of the bundle. Then, this prototype curve was transformed into subject native space using the transform computed using DTI-TK. For a given tract, streamline vertices are reparameterized to best match the prototype to allow for correspondence across streamlines at different cross-sections. Then, the average scalar parameter was computed for each group of vertices that matched the vertices of the reference, and the resulting along-bundle parameter maps were retained for subsequent statistical analysis.

2.7. Statistical analysis

For whole-tract analyses, males and females were combined because no significant differences were identified (Supplementary Table 2). To assess gross patterns of white matter tract development and provide overall tract summary parameters, the NDI, ODI, FA, RD and MD values were averaged over left and right sides for whole-tract analyses (e.g., Left ATR + Right ATR). In order to better localize the core of a tract, tract density was used to derive per tract weighted averages of NODDI parameters according to:

$$\bar{x} = \frac{\sum_{i=1}^n w_i x_i}{\sum_{i=1}^n w_i} \quad (2)$$

where n denotes the number of voxels within a tract and w_i and x_i are the number of streamlines passing through and the calculated parameter for the i th voxel within a tract, respectively, and \bar{x} is the weighted parameter average for a tract.

The relationship between tract parameter weighted averages and age for each bilateral whole-tract analysis were tested using linear, quadratic, logistic, Brody, von Bertalanffy, and negative exponential growth curve models. Model selection using Bayesian information criteria (BIC) was used to identify the curves that explained the most age-related variance in NODDI and DTI parameters. Exponential maturational patterns were described using Brody growth models. Brody growth models of the form:

$$parameter = \alpha - (\alpha - \beta)e^{-k \cdot age} \quad (3)$$

were fit to relate diffusion parameters and age using nonlinear least squares regression where α is the asymptote, β is the y-intercept, and k is the growth rate. Developmental timing was defined as the age at which a given parameter reaches 90% of its asymptotic value, and the degree of maturation was calculated as the percent change in parameter value at this terminal age. Standard errors and confidence intervals for the coefficients, terminal maturation age, and percent change for each tract in equation were calculated using bootstrap resampling with 5000 iterations using R. Linear regression was used to describe the relationship between ODI and age.

For along-tract analyses, Brody growth curves were fit at each point along the left and right tracts separately to quantify the relationship between regional parameter values and age. At each point, the age at 90% maturation was calculated. Bootstrap resampling was performed along each tract with 5000 iterations to obtain a confidence interval around the regional along-tract age estimates.

3. Results

Model selection using BIC showed that the Brody growth function provided the best fit model for NDI used in subsequent analyses (Supplementary Table 3).

3.1. Mean ODI changes with age

There were weak but significant correlations between age and ODI in the corticospinal tract, $\beta = -0.0013$, $t(102) = -2.66$, $p = .009$, forceps

major, $\beta = -0.0033$, $t(102) = -3.16$, $p = .002$, and inferior fronto-occipital fasciculus, $\beta = -0.0017$, $t(102) = -2.53$, $p = .013$, with ODI negatively associated with age in these regions (Fig. 2). No other major white matter tract showed age-related changes in mean tract ODI. When comparing across tracts, the corticospinal tract had the lowest average ODI ($M = 0.257$), while the cingulum had the highest average ODI ($M = 0.385$).

3.2. Mean NDI changes with age

Significant exponential changes, as measured with Brody growth curves, were observed in all bilateral tracts (Fig. 3). The mean terminal ages estimated from the Brody model for each tract ranged from childhood through adulthood (7.06–28.02 years, $M = 16.98$ years). Within the age range studied, the forceps minor reached terminal NDI maturation earliest ($M = 7.06$ years, $SE = 2.45$ years) and the inferior longitudinal fasciculus reached terminal NDI maturation latest ($M = 18.63$ years, $SE = 3.92$ years). Three tracts had terminal age estimates outside the age range sampled and include the inferior longitudinal fasciculus ($M = 19.45$ years, $SE = 7.01$ years), the uncinate fasciculus ($M = 19.65$ years, $SE = 10.1$ years) and the cingulum ($M = 28.02$, $SE = 15.02$) (Table 1). The uncinate fasciculus showed the smallest percent change in NDI from infancy through 18 years of age (65%), while the largest percent change in NDI was observed in the forceps minor (121%). Variance in terminal age estimates varied across tracts, with the smallest variance observed in the forceps minor ($SE = 2.45$ years) and the largest variance observed in the cingulum ($SE = 15.02$).

3.3. Mean DTI changes with age

The mean terminal age estimates for each tract using DTI parameters ranged from childhood through adulthood (FA: 3.54–24.77, $M = 13.21$ years; MD: 3.04–37.43, $M = 11.37$ years; RD: 2.36–26.04, $M = 10.23$ years) (Supplementary Figs. 1–3). The estimated terminal age for the cingulum with FA ($M = 24.77$ years) and the corticospinal tract with MD ($M = 37.43$ years) and RD ($M = 26.04$ years) were outside the age range sampled. For these tracts, bootstrapping yielded biologically implausible standard errors for the upper asymptote (α) coefficient and age to reach 90% of α . The forceps minor reached terminal maturation earliest and showed the largest percent change for FA ($M = 3.54$, $SE = 1.64$ years, 93%), MD ($M = 3.04$, $SE = 1.33$ years, 270%), and RD ($M = 2.36$, $SE = 1.28$ years, 66%). The forceps major showed the smallest percent change for FA (46%) and MD (71%), while the cingulum had the smallest percent change for RD (28%).

3.4. Developmental rate and timing of tract-specific NODDI changes

The regional variability of the mean ODI distribution and NDI, FA, MD and RD developmental rates within individual white matter tracts can be represented with a vector of measures sampled at equidistant points along the length of each tract. Average ODI varied along the lengths of the tract and tended to be higher in superficial tract segments compared to the core (Fig. 4). The ODI distribution along each tract did not noticeably differ from the contralateral tract. For the tracts explored, regional ODI was not significantly associated with age and could not be described using a growth curve.

Average NDI varied along the lengths of each tract. In the majority of tracts, the relationship between age and NDI at each point can be described with an exponential growth curve. However, a multitude of regions within the left and right cingulum did not show significant exponential growth of NDI with age and were excluded from the following analysis. Brody growth models applied to the resulting tracts demonstrated that the estimated age at terminal maturation varies along the length of each tract (Fig. 5). The estimated terminal ages in regions of the forceps major, bilateral superior longitudinal fasciculus and left inferior longitudinal fasciculus yielded unreliable age estimates outside

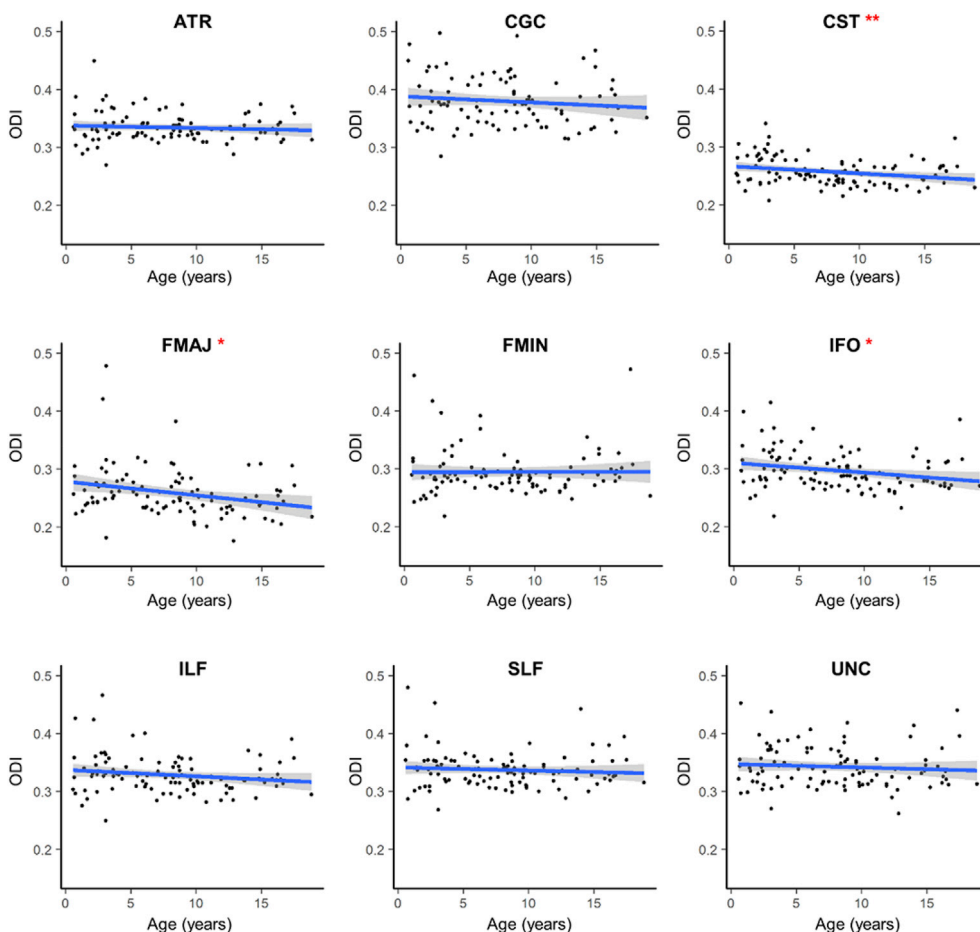


Fig. 2. Age-related changes in mean ODI for major white matter tracts.

ODI values are averaged across the left and right hemispheres for each tract. Regression line shows the best fit line relating age and ODI. Age was significantly and negatively associated with age in the CST, FMAJ and IFO only. * $p < .05$; ** $p < .01$.

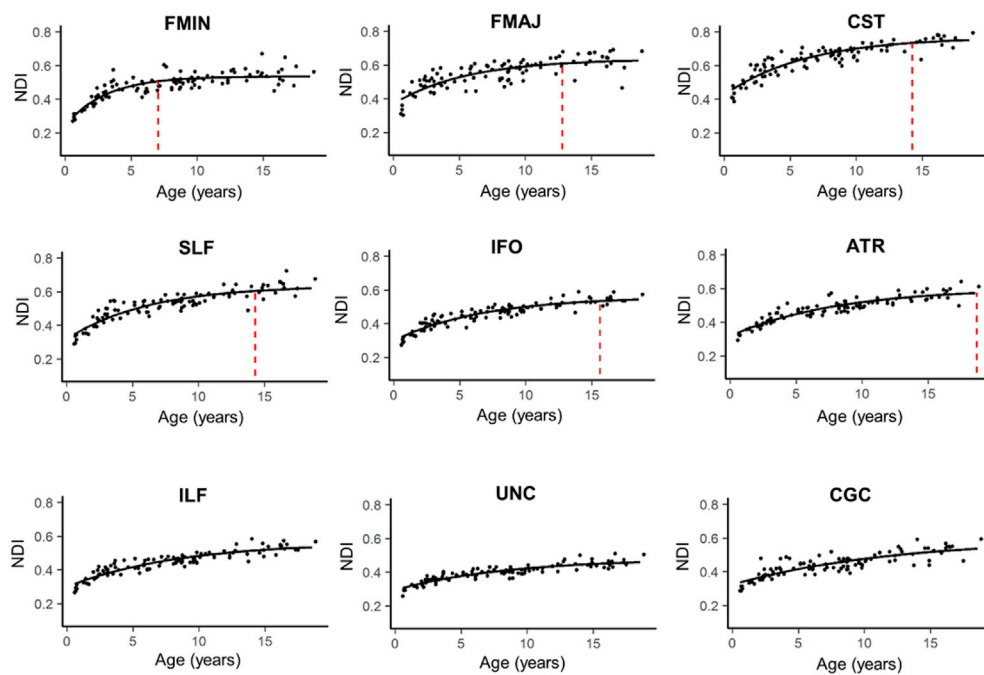


Fig. 3. Age-related NDI increases in major white matter tracts with exponential fits. NDI values are averaged across the left and right hemispheres for each tract. Maximum NDI plateau of each tract are marked by the vertical dotted red lines and plots are ordered according to how quickly the tract reaches the NDI plateau. The ILF, UNC and CGC are not marked because these tracts reach the NDI plateau outside the age range explored. Parameters for the exponential fits for each tract are presented in [Table 1](#).

Table 1

Description of NODDI parameters in bilateral whole-tract analyses. Exponential fits relating age and NDI for asymptote (α), y-intercept (β) and exponential time constant (k) parameters, and age where NDI reaches 90% of the asymptotic value (T_{exp}). For all estimated parameters, the standard error is provided (SE).

Tract	α (SE)	k (SE)	β (SE)	T_{exp} (SE)
ATR	0.606 (.023)	0.125 (0.021)	0.317 (.011)	18.68 (6.64)
CGC	0.614 (.121)	0.085 (0.030)	0.323 (.013)	28.02 (15.02)
CST	0.774 (.019)	0.160 (.026)	0.426 (.018)	14.24 (4.16)
FMAJ	0.640 (.023)	0.182 (.044)	0.367 (.024)	12.80 (9.28)
FMIN	0.538 (.009)	0.326 (.051)	0.243 (.026)	7.06 (2.45)
IFO	0.566 (.014)	0.144 (.021)	0.300 (.011)	18.63 (3.92)
ILF	0.567 (.023)	0.119 (.022)	0.299 (.010)	19.45 (7.01)
SLF	0.638 (.019)	0.165 (.027)	0.315 (.017)	14.29 (8.54)
UNC	0.486 (.020)	0.116 (.024)	0.295 (.008)	19.65 (10.10)

ATR, anterior thalamic radiation; CGC, cingulum; CST, corticospinal tract; FMAJ, forceps major; FMIN, forceps minor; IFO, inferior fronto-occipital fasciculus; ILF, inferior longitudinal fasciculus; SLF, superior longitudinal fasciculus; UNC, uncinete fasciculus.

the age range for this study. The estimated age to maximum NDI tends to be higher and more variable in the superficial white matter compared to the tract core. In general, regions that have younger terminal age estimates have smaller bootstrapped variance than regions that have older terminal age estimates. Overall, the left and right tracts showed similar patterns of maturation. Furthermore, the forceps minor and forceps major showed similar rates of maturation between the left and right hemispheres. However, left-right differences in maturational timing were observed in the superior longitudinal fasciculus. While a faster rate of NDI development was observed in the core of the left superior longitudinal fasciculus, a slower rate of change was observed in the frontal half of the right tract.

3.5. Developmental rate and timing of tract-specific DTI changes

The majority of tract segments showed exponential growth using FA, MD and RD and the estimated age at terminal maturation varies along the length of each tract (Supplementary Figs. 4-6). However, a multitude of tract regions for the microstructural parameters tested had poor exponential fits and were excluded from the analyses. These include the bilateral cingulum and forceps major with FA, MD and RD; and the corticospinal tract with MD and RD. With FA, unreliable estimates outside the age range sampled were observed in the bilateral corticospinal tract, inferior fronto-occipital fasciculus, inferior longitudinal fasciculus and superior longitudinal fasciculus and the right anterior thalamic radiation. Like NDI, the majority of the left and right tracts had similar patterns of exponential maturation, including the forceps minor. In general, major white matter tract regions reached their maximum values later for NDI and FA (between 10 and 30 years of age) compared to MD and RD (before the age of 10 years).

4. Discussion

The current study sought to characterize the maturation patterns of major white matter tracts in typical development from infancy through adolescence using NODDI. Using a semi-automated tractography approach, we demonstrate widespread age-related increases in tract NDI. NDI follows an exponential growth pattern and increases rapidly in infancy and young childhood followed by a plateau in adolescence. NDI represents the tissue volume fraction occupied by neurites, such as axons and dendrites, and is considered a proxy for neurite density (Sepehrband et al., 2015). Postmortem evidence suggests that increases in neurite density, through myelination and axon packing, is a prominent feature of white matter development in childhood (Benes, 1989; Miller et al., 2012), and this is supported by findings that NDI accounts for more age-related variance compared to DTI (Genc et al., 2017). Together, these results demonstrate NDI's sensitivity to developmentally relevant

processes. ODI, a measure of axonal orientation variance, was not significantly associated with age in the majority of white matter tracts, however weak negative correlations were observed between ODI and age in the corticospinal tract, forceps major, and inferior fronto-occipital fasciculus. Our results are largely in line with previous cross-sectional findings of positive correlations between NDI and age and little or no correlation between ODI and age (Chang et al., 2015; Geeraert et al., 2019; Mah et al., 2017), suggesting this period is marked by progressive increases in neurite density that are not accompanied by changes in geometric complexity.

Previous studies shows that DTI metrics are sensitive to developmental processes, however the relative contribution of various structural features is unclear. While there is evidence that RD can be sensitive to myelination (Song et al., 2002), it can also reflect fiber organization (Wheeler-Kingshott and Cercignani, 2009). Additionally, FA is negatively correlated with ODI and expresses a weak positive association with NDI (Zhang et al., 2012). Consequently, orientation dispersion and, to a lesser extent, neurite density influence FA estimates. It is therefore important to interpret DTI results in the context of development with caution.

The magnitude and timing of neurite density maturation, as implied by cross-sectional changes of NDI with age, can be obtained for each white matter tract using the growth curve fit for that particular white matter tracts. Significant variability was observed in the developmental trajectories of whole-tract averages, with callosal fibers developing earlier than association tracts. The age where maximum NDI is achieved can be defined as the time to reach 90% of asymptote estimated from the individual tract growth curves. The forceps minor and forceps major, callosal connections critical for interhemispheric communication (Aboitiz and Montiel, 2003), show the earliest changes of NDI with age, reaching terminal NDI before 7 years of age. In particular, the forceps minor, which connects bilateral fronto-temporal regions through the genu of the corpus callosum, demonstrates the earliest and most rapid NDI maturation, with NDI more than doubling by the time it reaches its developmental plateau. Diffusion parameters similarly show the forceps minor develops earlier than other tracts in this study, however the developmental plateau estimated using FA, MD and RD is younger (~3 years) compared to NODDI (~7 years). These results are in agreement with previous findings demonstrating early maturation of callosal projections using FA as a measure of microstructure (Cancelliere et al., 2013; Chen et al., 2016; Krogsrud et al., 2016; Lebel et al., 2019, 2008). NODDI studies have demonstrated sparse growth (Chang et al., 2015; Geeraert et al., 2019) or small decreases (Mah et al., 2017) of NDI with age in the forceps minor, which may be attributed to the older age ranges used in their samples (children older than 6 years of age).

The corticospinal tract, a projection fiber critical for voluntary motor control, reached mature NDI by mid-adolescence. Association tracts projecting to the frontal lobes developed later and include the fronto-temporal fibers of the superior longitudinal fasciculus, the fronto-occipital fibers of the inferior fronto-occipital fasciculus and the thalamo-cortical projections of the anterior thalamic radiation. The inferior longitudinal fasciculus and fronto-temporal fibers of the uncinete fasciculus and cingulum mature much later and reach peak NDI after 18 years of age. The developmental timing as measured with diffusion tensor parameters partially agree with those estimated with NDI. The anterior thalamic radiation and cingulum similarly develops later in adolescence and adulthood with FA. These results are consistent with a protracted pattern of frontal gray and white matter maturation observed in several neurodevelopment diffusion studies (Asato et al., 2010; Chen et al., 2016; Dean et al., 2015; Lebel et al., 2008; Tamnes et al., 2010). In contrast to the relatively early development of NDI in the corticospinal tract, MD and RD shows a much more protracted developmental trajectory of this fiber bundle with the plateau reached well into adulthood. This is not entirely unexpected as DTI and NODDI parameters are sensitized to different microstructural phenomena that likely follow distinct developmental time courses (Tau and Peterson, 2010). Because there is evidence that regional developmental patterns in white matter

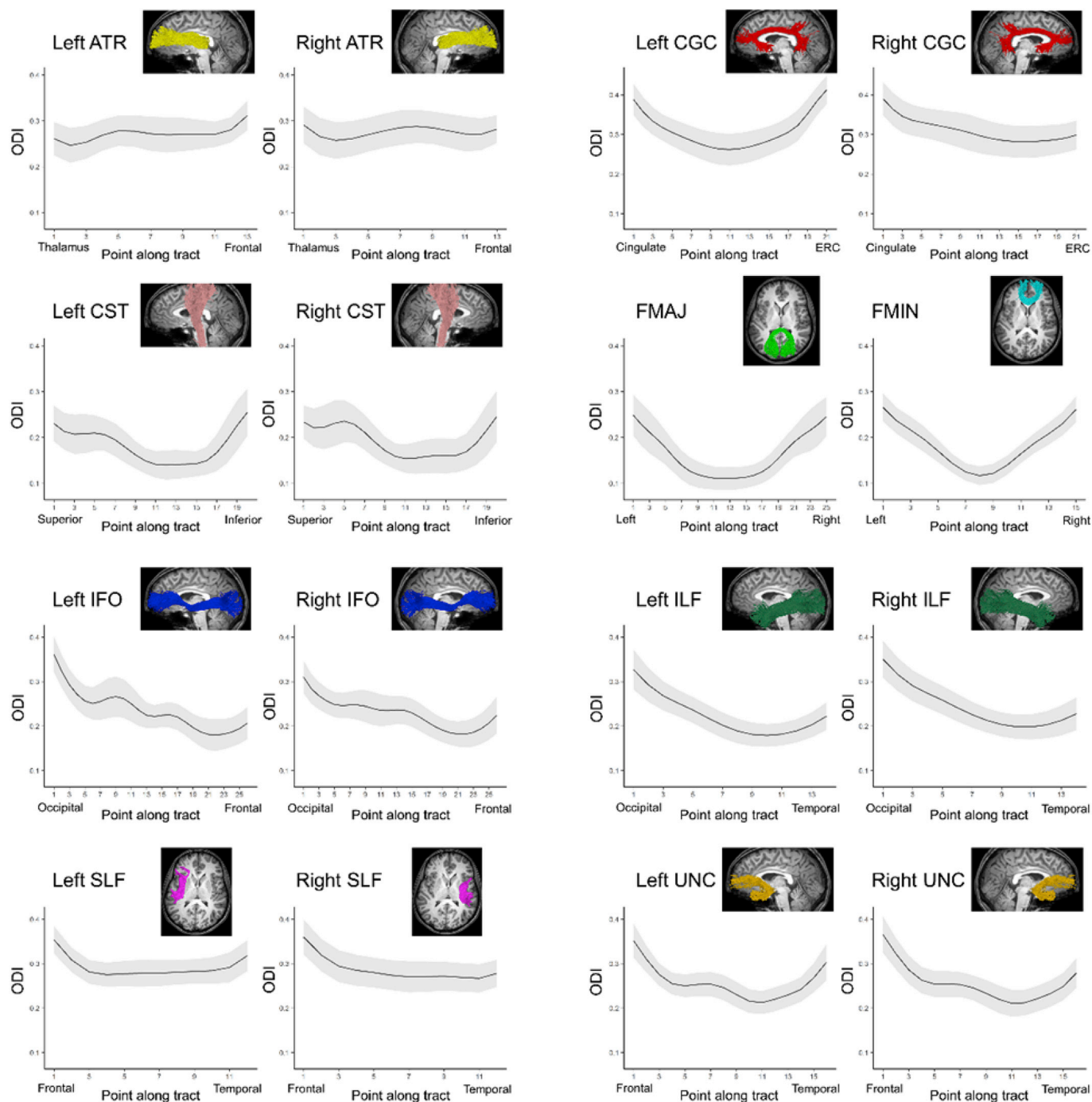


Fig. 4. Mean ODI along the length of major white matter tracts.

The average ODI is plotted for each point along bilateral major white matter tracts. The shaded region indicates the standard deviation.

are linked to changes in behavior (Klarborg et al., 2013; Peters et al., 2014; Ullman et al., 2014; Ullman and Klingberg, 2016; Yeatman et al., 2012a), the variability in white matter development could provide important clues as to the concomitant development of higher-level cognitive functions. These results are critical for understanding the timing of white matter microstructural changes that shape emerging cognition.

While analyses of whole tract changes can inform the relative ordering of white matter tract maturation, this approach may oversimplify white matter developmental processes by assuming NODDI parameters change in unison across whole tracts. Along-tract analyses allow for the quantification of tissue properties at discrete locations along the

path of white matter fibers. Using this approach, we demonstrate that aging does not affect major white matter tract NDI uniformly. This is consistent with previous results showing regional patterns of white matter maturation using diffusion parameters (Chen et al., 2016; Colby et al., 2011; Johnson et al., 2014; Yeatman et al., 2012b). In the present study, superficial white matter components of the tracts tended to reach terminal NDI at older ages and with more variance compared to the core of the tracts, as evidenced with the forceps minor, left superior longitudinal fasciculus, and right corticospinal tract. The variability may be due in part to partial volume effects at the interface of gray and white matter. However, as short, small-diameter fibers that provide intra-cortical connections, superficial white matter has been shown to undergo

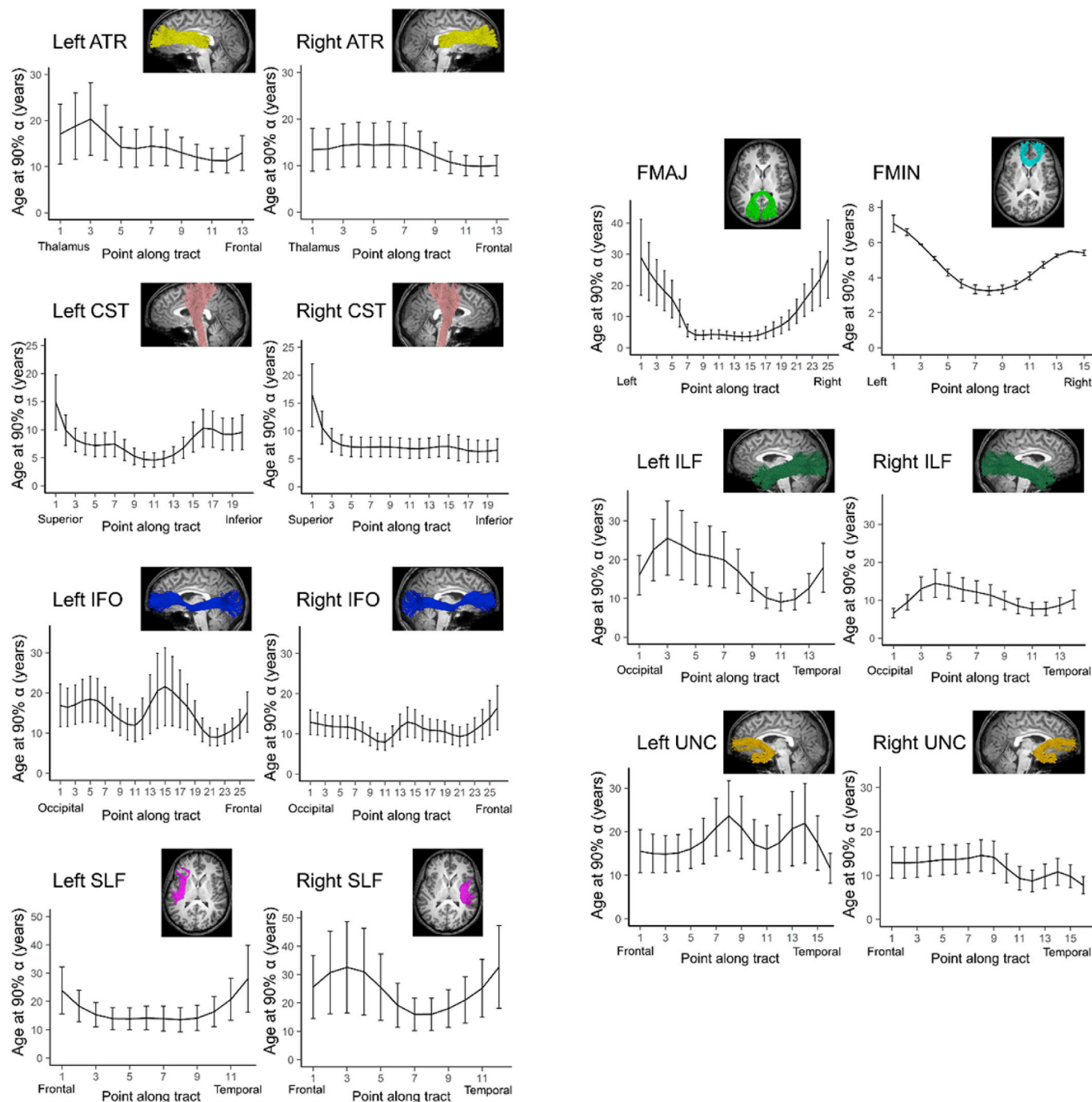


Fig. 5. Developmental timing of NDI maturation along white matter tracts.

The estimated age where NDI reaches 90% maturation is plotted for each point along the length of bilateral major white matter tracts. Error bars indicate the bootstrapped 99% confidence interval. The along-tract development of the CGC is not included due to poor fitting.

myelination later than deep white matter (Wu et al., 2016, 2014). ODI also varies along the length of major white matter tracts, which can be explained by local differences in directional coherence, including curvature, crossing fibers, and the entrance and exit of smaller axon bundles that intersect with the tract. Different rates of NDI maturation may be explained by the heterochronous development of white matter (Miller et al., 2012), as the rate of myelination can differ among white matter regions.

While the forceps minor reached terminal maturation earliest on average, along-tract analyses reveal the fibers passing through the genu of the corpus callosum develop earlier than the rest of the tract using NDI,

FA, MD and RD. These findings are supported by previous studies on the development of diffusion parameters demonstrate early rapid growth localized to the genu (Chen et al., 2016; Johnson et al., 2014). The agreement among NODDI and DTI parameters could be attributed to the coherent organization of callosal fibers that result in reduced diffusion signal contamination (Genc et al., 2017). These estimates may therefore reflect true microstructural processes that are not obscured by crossing or complex fiber orientations. Our results suggest the early maturation of the genu observed with DTI parameters and NDI, which models the full spectrum of fiber orientations, is due to an increase in neurite density via axonal packing and myelination. The early maturation of the corpus

callosum relative to the rest of the brain may be due to its role in inter-hemispheric communication, which allows for functional integration, hemispheric specialization, and information transfer between homologous cortical areas (Aboitiz and Montiel, 2003), and there is some evidence supporting a general central-to-peripheral maturational gradient in the brain (Deoni et al., 2012; Yakovlev and Lecours, 1967).

NDI maturational patterns for other tracts were not always in agreement with DTI parameters. In the corticospinal tract, which projects from the motor regions in the frontal lobule to the brainstem, NDI and FA show opposite developmental changes. The developmental timing in the superficial white matter adjacent to precentral regions is much slower with NDI compared to FA. At the level of the midbrain, however, the development of FA is prolonged and highly variable while that of NDI is more stable at approximately 10 years of age. The inferior corticospinal tract contains crossing fibers and decussations and it is possible that the large variability observed with FA may be due to diffusion signal contamination. While the majority of regions along the white matter tracts demonstrated exponential age-related change in diffusion microstructural parameters, the growth models did not always provide a good fit and this was observed more frequently with the DTI measures. This is consistent with other studies that showed subsets of white matter tracts exhibiting exponential changes using a surface-based model (Chen et al., 2016). Regions with poor exponential fits may have achieved terminal maturation by birth, undergo a protracted maturational process that is observed later than our sample allowed, or may be better described with a linear fit (Chen et al., 2016; Lebel et al., 2008).

A main limitation of any study characterizing developmental trajectories is that conclusions and interpretations highly depend on the modelling technique and age range sampled. Lebel et al. (2019) recently demonstrated that the curve fitting and estimated rate of developmental changes differed depending on the age range used, particularly in fast developing tracts (Lebel et al., 2019). In the present study, inclusion of infants and exclusion of participants older than 18 years of age may result in a selection bias that can influence the estimated age-related trajectories. While exponential growth curves provided the best fit according to BIC and offers significant improvements over linear fits (Lebel et al., 2008; Taki et al., 2013; Tamnes et al., 2010), this model may not be appropriate over a different or expanded age range. Inclusion of infants provides the ability to capture the rapid early increases in microstructural parameters that will influence the curve fitting and estimated growth rate (Hermoye et al., 2006; McGraw et al., 2002; Oishi et al., 2013). Furthermore, it is possible that the asymptote has not been achieved by 18 years of age in some tracts, which would result in an underestimation of the age at the developmental plateau. In fact, lifespan studies of white matter development show myelination continues well into adulthood (Hasan et al., 2010; Lebel et al., 2012; Sowell et al., 2003; Westlye et al., 2010) and diffusion studies demonstrate prolonged maturation of white matter FA (Chen et al., 2016; Lebel et al., 2008). Therefore, interpretation of results and comparison with other developmental studies should be done with caution.

Another limitation of the present study was the cross-sectional nature of the design. Cross-sectional studies can capture relationships between microstructural parameters and age, however they are heavily influenced by inter-subject variability. Future longitudinal studies of white matter maturation using NODDI models and along-tract analyses can provide the added benefit of providing information about microstructural changes within subjects to more accurately define white matter developmental trajectories.

The biophysical interpretation of NODDI parameters should be considered with caution because, like all models, certain assumptions are made that may oversimplify tissue microstructure. The minimal model employed by NODDI makes it applicable to a wide variety of clinical and research studies, but these simplifications can also result in biases and uncertainties in parameter estimation (Jelescu et al., 2016). For example, NODDI fixes intra- and extra-axonal diffusivities to *a priori* values. This may bias the results because some biological variability is expected that

may change across developmental stages (Jelescu et al., 2014; Kunz et al., 2014). A recent study demonstrated that the default intrinsic parallel diffusivity used in the NODDI model is not optimal in infants as young as 1 month old. In order to overcome this limitation, we only included infants older than 7 months of age (Guerrero et al., 2019). We conducted a similar post-hoc analysis in our data and found the default intrinsic parallel diffusivity to be optimal in deep white matter in infants and toddlers older than 1 year of age. For infants between 6 months and 1 year of age, however, we found that the optimal intrinsic parallel diffusivity varies across different tracts, and the default value was within the range of optimal values. Previous studies have demonstrated that intrinsic parallel diffusivities vary across the brain in normative adult populations (Kaden et al., 2016). Therefore, this problem is not unique to infant populations. While it is tempting to consider the intrinsic parallel diffusivity as a free parameter to be estimated from the diffusion signal itself, this can lead to unstable estimates of other parameters (Jelescu et al., 2016). Future studies should further explore the influence of regional variation of microscopic diffusivity properties in the brain in order to better assess the validity of multi-compartment models such as NODDI. Another limitation related to data modeling is the nature of the CMIND diffusion MRI data, which had slightly different scanning sequence parameters between shells. We used a normalization procedure similar to previous reports (Genc et al., 2018, 2017; Claire E Kelly et al., 2016; Owen et al., 2014), which can possibly account for intensity differences, assuming there are only negligible differences in T1 and T2 relaxation among tissue compartments. Nevertheless, care should be taken when directly comparing specific parameter estimates obtained using other sequences, as there may be subtle biases that remain after normalization.

In conclusion, this study used NODDI parameters sensitized to microstructural features to investigate the magnitude and timing of maturational changes in major white matter tracts from infancy through adolescence. Along-tract analyses provide a framework to uncover spatial distributions of microstructural age effects within white matter tracts, and our results indeed demonstrate regional patterns of NDI timing within and across tracts. Additionally, ODI did not show significant associations with age, suggesting that white matter development over this time period is attributed to increases in neurite density, likely through increased axonal packing and myelination. Overall, our results demonstrate the utility of NODDI models for characterizing the heterochronous developmental patterns of white matter microstructure. These results add to the growing body of research aiming to characterize how changes in brain structure contribute to complex cognitive function, as these efforts are necessary for ultimately understanding the origins of developmental disability.

Data availability

All data used in this study is available at the Cincinnati MR Imaging of Neurodevelopment (C-MIND) database (<http://research.cchmc.org/c-mind>).

CRediT authorship contribution statement

Kirsten M. Lynch: Writing - original draft, Writing - review & editing, Conceptualization, Visualization, Methodology. **Ryan P. Cabeen:** Writing - review & editing, Software, Methodology. **Arthur W. Toga:** Supervision. **Kristi A. Clark:** Supervision, Writing - review & editing.

Acknowledgements

The authors would like to thank Farshid Sepehrband, Scott Holland, and members of the Connectivity and Network Development group for their comments, support, and assistance during this project.

Appendix A. Supplementary data

Supplementary data to this article can be found online at <https://doi.org/10.1016/j.neuroimage.2020.116672>.

Funding

This work was supported by the Eunice Kennedy Shriver National Institute of Child Health and Human Development (R00HD065832), the National Institute of Biomedical Imaging and Bioengineering (P41EB015922 and U54EB020406), the National Institute of Neurological Disorders and Stroke (R21NS091586), and the National Institute of Mental Health (R01MH094343). This work was partially supported by a NARSAD Young Investigator Award. Data collection and sharing for this project was funded by The Cincinnati MR Imaging of Neurodevelopment study (C-MIND) (supported by the National Institute of Child Health and Human Development Grant HHSN275200900018C).

References

- Assaf, Y., Cohen, Y., 2000. Assignment of the water slow-diffusing component in the central nervous system using q-space diffusion MRS: implications for fiber tract imaging. *Magn. Reson. Med.* 43, 191–199. [https://doi.org/10.1002/\(SICI\)1522-2594\(200002\)43:2<191::AID-MRM5>3.0.CO;2-B](https://doi.org/10.1002/(SICI)1522-2594(200002)43:2<191::AID-MRM5>3.0.CO;2-B).
- Seppehrband, F., Clark, K.A., Ullmann, J.F.P., Kurniawan, N.D., Leanage, G., Reutens, D.C., Yang, Z., 2015. Brain tissue compartment density estimated using diffusion-weighted MRI yields tissue parameters consistent with histology. *Hum. Brain Mapp.* <https://doi.org/10.1002/hbm.22872>, 00, n/a-n/a.
- Aboitiz, F., Montiel, J., 2003. One hundred million years of interhemispheric communication: the history of the corpus callosum. *Braz. J. Med. Biol. Res.* 36, 409–420. <https://doi.org/10.1590/S0100-879X2003000400002>.
- ACR, 2004. MRI Quality Control Manual, Vol P-MRQC. American College of Radiology, Reston, VA.
- Asato, M.R., Terwilliger, R., Woo, J., Luna, B., 2010. White matter development in adolescence: a DTI study. *Cerebr. Cortex* 20, 2122–2131. <https://doi.org/10.1093/cercor/bhp282>.
- Beaulieu, C., 2002. The basis of anisotropic water diffusion in the nervous system - a technical review. *NMR Biomed.* 15, 435–455. <https://doi.org/10.1002/nbm.782>.
- Beaulieu, C., 2009. The biological basis of diffusion anisotropy. In: Johansen-Berg, H., Behrens, T.E.J. (Eds.), *Diffusion MRI: from Quantitative Measurement to In-Vivo Neuroanatomy*. Academic Press, pp. 105–129. <https://doi.org/10.1016/B978-0-12-396460-1.00008-1>.
- Behrens, T.E.J., Berg, H.J., Jbabdi, S., Rushworth, M.F.S., Woolrich, M.W., 2007. Probabilistic diffusion tractography with multiple fibre orientations: what can we gain? *Neuroimage* 34, 144–155. <https://doi.org/10.1016/j.neuroimage.2006.09.018>.
- Benes, F., 1989. Myelination of cortical-hippocampal relays during late adolescence. *Schizophr. Bull.* 15, 585–593.
- Cabeen, R.P., Bastin, M.E., Laidlaw, D.H., 2016. Kernel regression estimation of fiber orientation mixtures in diffusion MRI. *Neuroimage* 127, 158–172. <https://doi.org/10.1016/j.neuroimage.2015.11.061>.
- Cabeen, R.P., Laidlaw, D.H., Toga, A.W., 2018. Quantitative Imaging Toolkit: Software for Interactive 3D Visualization, Data Exploration, and Computational Analysis of Neuroimaging Datasets.
- Cancelliere, A., Mangano, F.T., Air, E.L., Jones, B.V., Altaye, M., Rajagopal, A., Holland, S.K., Hertzler, D.A., Yuan, W., 2013. DTI values in key white matter tracts from infancy through adolescence. *Am. J. Neuroradiol.* 34, 1443–1449. <https://doi.org/10.3174/ajnr.A3350>.
- Catani, M., de Schotten, M.T., 2012. *Atlas of Human Brain Connections*. Oxford University Press.
- Catani, M., Howard, R.J., Pajevic, S., Jones, D.K., 2002. Virtual in vivo interactive dissection of white matter fasciculi in the human brain. *Neuroimage* 17, 77–94. <https://doi.org/10.1006/nimg.2002.1136>.
- Chang, Y.S., Owen, J.P., Pojman, N.J., Thieu, T., Bukshpun, P., Wakahiro, M.L.J., Berman, J.I., Roberts, T.P.L., Nagarajan, S.S., Sherr, E.H., Mukherjee, P., 2015. White matter changes of neurite density and fiber orientation dispersion during human brain maturation. *PLoS One* 10, e0123656. <https://doi.org/10.1371/journal.pone.0123656>.
- Chen, Z., Zhang, H., Yushkevich, P.A., Liu, M., Beaulieu, C., 2016. Maturation along white matter tracts in human brain using a diffusion tensor surface model tract-specific analysis. *Front. Neuroanat.* 10, 1–18. <https://doi.org/10.3389/fnana.2016.00009>.
- Clayden, J.D., Jentschke, S., Muñoz, M., Cooper, J.M., Chadwick, M.J., Banks, T., Clark, C.A., Vargha-Khadem, F., 2012. Normative development of white matter tracts: similarities and differences in relation to age, gender, and intelligence. *Cerebr. Cortex* 22, 1738–1747. <https://doi.org/10.1093/cercor/bhr243>.
- Colby, J.B., Van Horn, J.D., Sowell, E.R., 2011. Quantitative in vivo evidence for broad regional gradients in the timing of white matter maturation during adolescence. *Neuroimage* 54, 25–31. <https://doi.org/10.1016/j.neuroimage.2010.08.014>.
- Colby, J.B., Soderberg, L., Lebel, C., Dinov, I.D., Thompson, P.M., Sowell, E.R., 2012. Along-tract statistics allow for enhanced tractography analysis. *Neuroimage* 59, 3227–3242. <https://doi.org/10.1016/j.neuroimage.2011.11.004>.
- Counsell, S.J., Zhang, H., Hughes, E., Steele, H., Tusor, N., Ball, G., Makropoulos, A., Alexander, D.C., Hajnal, J.V., Edwards, D., 2014. In vivo assessment of neurite density in the preterm brain using diffusion magnetic resonance imaging. *Proc. Int. Soc. Mag. Reson. Med.* 22.
- Dean, D.C., O'Muircheartaigh, J., Dirks, H., Waskiewicz, N., Walker, L., Doernberg, E., Piryatinsky, I., Deoni, S.C.L., 2015. Characterizing longitudinal white matter development during early childhood. *Brain Struct. Funct.* 220, 1921–1933. <https://doi.org/10.1007/s00429-014-0763-3>.
- Deoni, S.C.L., Dean, D.C., Muircheartaigh, J.O., Dirks, H., Jerskey, B.A., 2012. Investigating white matter development in infancy and early childhood using myelin water fraction and relaxation time mapping. *Neuroimage* 63, 1038–1053. <https://doi.org/10.1016/j.neuroimage.2012.07.037>.
- Eluvathingal, T.J., Hasan, K.M., Kramer, L., Fletcher, J.M., Ewing-Cobbs, L., 2007. Quantitative diffusion tensor tractography of association and projection fibers in normally developing children and adolescents. *Cerebr. Cortex* 17, 2760–2768. <https://doi.org/10.1093/cercor/bhm003>.
- Geraert, B.L., Lebel, R.M., Lebel, C., 2019. A multiparametric analysis of white matter maturation during late childhood and adolescence. *Hum. Brain Mapp.* <https://doi.org/10.1002/hbm.24706>. Epub ahead.
- Genc, S., Malpas, C.B., Holland, S.K., Beare, R., Silk, T.J., 2017. Neurite density index is sensitive to age related differences in the developing brain. *Neuroimage* 148, 373–380. <https://doi.org/10.1016/j.neuroimage.2017.01.023>.
- Genc, S., Malpas, C.B., Ball, G., Silk, T.J., Seal, M.L., 2018. Age, sex, and puberty related development of the corpus callosum: a multi-technique diffusion MRI study. *Brain Struct. Funct.* 223, 2753–2765. <https://doi.org/10.1007/s00429-018-1658-5>.
- Gogtay, N., Giedd, J.N., Lusk, L., Hayashi, K.M., Greenstein, D., Vaituzis, A.C., Iii, T.F.N., Herman, D.H., Clasen, L.S., Toga, A.W., Rapoport, J.L., Thompson, P.M., 2004. Dynamic mapping of human cortical development during childhood through early adulthood. *Proc. Natl. Acad. Sci. Unit. States Am.* 101, 8174–8179.
- Goodlett, C.B., Fletcher, P.T., Gilmore, J.H., Gerig, G., 2009. Group analysis of DTI fiber tract statistics with application to neurodevelopment. *Neuroimage* 45, S133–S142. <https://doi.org/10.1016/j.neuroimage.2008.10.060>.
- Guerrero, J.M., Adluru, N., Bendlin, B.B., Goldsmith, H.H., Schaefer, S.M., Davidson, R.J., Keskemeti, S.R., Zhang, H., Alexander, A.L., 2019. Optimizing the intrinsic parallel diffusivity in NODDI: an extensive empirical evaluation. *PLoS One* 14, 1–17. <https://doi.org/10.1371/journal.pone.0217118>.
- Hasan, K.M., Kamali, A., Ewing-cobbs, J.M.F.L., 2010. Quantification of the Spatiotemporal Microstructural Organization of the Human Brain Association, Projection and Commissural Pathways across the Lifespan Using Diffusion Tensor Tractography, pp. 361–373. <https://doi.org/10.1007/s00429-009-0238-0>.
- Hermoye, L., Saint-Martin, C., Cosnard, G., Lee, S.-K., Kim, J., Nassogne, M.-C., Menten, R., Clapuyt, P., Donohue, P.K., Hua, K., Wakana, S., Jiang, H., van Zijl, P.C.M., Mori, S., 2006. Pediatric diffusion tensor imaging: normal database and observation of the white matter maturation in early childhood. *Neuroimage* 29, 493–504. <https://doi.org/10.1016/j.neuroimage.2005.08.017>.
- Holland, S., Schmithorst, V.J., Wagner, M., Lee, G., Rajagopal, A., Sroka, M., Felicelli, N., Rupert, A., Clark, K., Toga, A., Freund, L., 2015. The C-MIND project: normative MRI and behavioral data from children from birth to 18 years. In: *Proceedings of the 21st Annual Meeting of the Organization for Human Brain Mapping*. OHBM, Honolulu, HA.
- Huttenlocher, P.R., 1979. Synaptic density in human frontal cortex - developmental changes and effects of aging. *Brain Res.* 163, 195–205. [https://doi.org/10.1016/0006-8993\(79\)90349-4](https://doi.org/10.1016/0006-8993(79)90349-4).
- Imperati, D., Colcombe, S., Kelly, C., Di Martino, A., Zhou, J., Castellanos, F.X., Milham, M.P., 2011. Differential development of human brain white matter tracts. *PLoS One* 6, e23437. <https://doi.org/10.1371/journal.pone.0023437>.
- Jelescu, I.O., Veraart, J., Adisetiyo, V., Milla, S., Novikov, D.S., Fieremans, E., 2014. One diffusion acquisition and different white matter models: how does microstructure change in human early development based on WMTI and NODDI? *Neuroimage* 107, 242–256. <https://doi.org/10.1016/j.neuroimage.2014.12.009>.
- Jelescu, I.O., Veraart, J., Fieremans, E., Novikov, D.S., 2016. Degeneracy in model parameter estimation for multi-compartmental diffusion in neuronal tissue. *NMR Biomed.* 29, 33–47. <https://doi.org/10.1002/nbm.3450>.
- Jenkinson, M., Bannister, P., Brady, M., Smith, S., 2002. Improved optimization for the robust and accurate linear registration and motion correction of brain images. *Neuroimage* 17, 825–841. [https://doi.org/10.1016/S1053-8119\(02\)91132-8](https://doi.org/10.1016/S1053-8119(02)91132-8).
- Johnson, R.T., Yeatman, J.D., Wandell, B.A., Buonocore, M.H., Amaral, D.G., Nordahl, C.W., 2014. Diffusion properties of major white matter tracts in young, typically developing children. *Neuroimage* 88, 143–154. <https://doi.org/10.1016/j.neuroimage.2013.11.025>.
- Jones, D.K., Cercignani, M., 2010. Twenty-five pitfalls in the analysis of diffusion MRI data. *NMR Biomed.* 23, 803–820. <https://doi.org/10.1002/nbm.1543>.
- Jones, D.K., Knösche, T.R., Turner, R., 2013. White matter integrity, fiber count, and other fallacies: the do's and don'ts of diffusion MRI. *Neuroimage* 73, 239–254. <https://doi.org/10.1016/j.neuroimage.2012.06.081>.
- Kaden, E., Kelm, N.D., Carson, R.P., Does, M.D., Alexander, D.C., 2016. Multi-compartment microscopic diffusion imaging. *Neuroimage* 139, 346–359. <https://doi.org/10.1016/j.physbeh.2017.03.040>.
- Kaiser, D., Leach, J., Vannest, J., Schapiro, M., Holland, S., 2015. Unanticipated findings in pediatric neuroimaging research: prevalence of abnormalities and process for reporting and clinical follow-up. *Brain Imag. Behav.* 9, 32–42. <https://doi.org/10.1007/s11682-014-9327-7>.

- Kelly, Claire E., Thompson, D.K., Chen, J., Leemans, A., Adamson, C.L., Inder, T.E., Cheong, J.L.Y., Doyle, L.W., Anderson, P.J., 2016. Axon density and axon orientation dispersion in children born preterm. *Hum. Brain Mapp.* 37, 3080–3102. <https://doi.org/10.1002/hbm.23227>.
- Klarborg, B., Skak Madsen, K., Vestergaard, M., Skimminge, A., Jernigan, T.L., Baaré, W.F.C., 2013. Sustained attention is associated with right superior longitudinal fasciculus and superior parietal white matter microstructure in children. *Hum. Brain Mapp.* 34, 3216–3232. <https://doi.org/10.1002/hbm.22139>.
- Kodiweera, C., Alexander, A.L., Harezlak, J., McAllister, T.W., Wu, Y.-C., 2015. Age effects and sex differences in human brain white matter of young to middle-aged adults: a DTI, NODDI, and q-space study. *Neuroimage*. <https://doi.org/10.1016/j.neuroimage.2015.12.033>.
- Krogsrud, S.K., Fjell, A.M., Tamnes, C.K., Grydeland, H., Mork, L., Due-Tønnessen, P., Bjørnerud, A., Sampaio-Baptista, C., Andersson, J., Johansen-Berg, H., Walhovd, K.B., 2016. Changes in white matter microstructure in the developing brain—A longitudinal diffusion tensor imaging study of children from 4 to 11 years of age. *Neuroimage* 124, 473–486. <https://doi.org/10.1016/j.neuroimage.2015.09.017>.
- Kunz, N., Zhang, H., Vasung, L., O'Brien, K.R., Assaf, Y., Lazeyras, F., Alexander, D.C., Hüppi, P.S., 2014. Assessing white matter microstructure of the newborn with multi-shell diffusion MRI and biophysical compartment models. *Neuroimage* 96, 288–299. <https://doi.org/10.1016/j.neuroimage.2014.03.057>.
- Lebel, C., Beaulieu, C., 2011. Longitudinal development of human brain wiring continues from childhood into adulthood. *J. Neurosci.* 31, 10937–10947. <https://doi.org/10.1523/JNEUROSCI.5302-10.2011>.
- Lebel, C., Walker, L., Leemans, A., Phillips, L., Beaulieu, C., 2008. Microstructural maturation of the human brain from childhood to adulthood. *Neuroimage* 40, 1044–1055. <https://doi.org/10.1016/j.neuroimage.2007.12.053>.
- Lebel, C., Caverhill-Godkewitsch, S., Beaulieu, C., 2010. Age-related regional variations of the corpus callosum identified by diffusion tensor tractography. *Neuroimage* 52, 20–31. <https://doi.org/10.1016/j.neuroimage.2010.03.072>.
- Lebel, C., Gee, M., Camicioli, R., Wielar, M., Martin, W., Beaulieu, C., 2012. Diffusion tensor imaging of white matter tract evolution over the lifespan. *Neuroimage* 60, 340–352. <https://doi.org/10.1016/j.neuroimage.2011.11.094>.
- Lebel, C., Treit, S., Beaulieu, C., 2019. A review of diffusion MRI of typical white matter development from early childhood to young adulthood. *NMR Biomed.* 32, e3778 <https://doi.org/10.1002/nbm.3778>.
- Mah, A., Geeraert, B., Lebel, C., 2017. Detailing neuroanatomical development in late childhood and early adolescence using NODDI. *PLoS One* 12, 1–16. <https://doi.org/10.1371/journal.pone.0182340>.
- Matsuzawa, J., Matsui, M., Konishi, T., Noguchi, K., Gur, R.C., Bilker, W., Miyawaki, T., 2001. Age-related volumetric changes of brain gray and white matter in healthy infants and children. *Cerebr. Cortex* 11, 335–342. <https://doi.org/10.1093/cercor/11.4.335>.
- McGraw, P., Liang, L., Provenzale, J.M., 2002. Evaluation of normal age-related changes in anisotropy during infancy and childhood as shown by diffusion tensor imaging. *Am. J. Roentgenol.* 179, 1515–1522. <https://doi.org/10.2214/ajr.179.6.1791515>.
- Miller, D.J., Duka, T., Stimpson, C.D., Schapiro, S.J., Baze, W.B., McArthur, M.J., Fobbs, A.J., Sousa, A.M.M., Sestan, N., Wildman, D.E., Lipovich, L., Kuzawa, C.W., Hof, P.R., Sherwood, C.C., 2012. Prolonged myelination in human neocortical evolution. *Proc. Natl. Acad. Sci. U.S.A.* 109, 16480–16485. <https://doi.org/10.1073/pnas.1117943109>.
- Oishi, K., Faria, A.V., Yoshida, S., Chang, L., Mori, S., 2013. Quantitative evaluation of brain development using anatomical MRI and diffusion tensor imaging. *Int. J. Dev. Neurosci.* 31, 512–524. <https://doi.org/10.1016/j.ijdevneu.2013.06.004>.
- Owen, J.P., Chang, Y.S., Pojman, N.J., Bukshpun, P., Wakahiro, M.L.J., Marco, E.J., Berman, J.I., Spiro, J.E., Chung, W.K., Buckner, R.L., Roberts, T.P.L., Nagarajan, S.S., Sherr, E.H., Mukherjee, P., for the Simons VIP Consortium, 2014. Aberrant white matter microstructure in children with 16p11.2 deletions. *J. Neurosci.* 34, 6214–6223. <https://doi.org/10.1523/JNEUROSCI.4495-13.2014>.
- Peters, B.D., Ikuta, T., Derosse, P., John, M., Burdick, K.E., Gruner, P., Prendergast, D.M., Szeszko, P.R., Malhotra, A.K., 2014. Age-related differences in white matter tract microstructure are associated with cognitive performance from childhood to adulthood. *Biol. Psychiatr.* 75, 248–256. <https://doi.org/10.1016/j.biopsych.2013.05.020>.
- Pierpaoli, C., Basser, P.J., 1996. Toward a quantitative assessment of diffusion anisotropy. *Magn. Reson. Med.* 36, 893–906. <https://doi.org/10.1002/mrm.1910360612>.
- Rice, D., Barone, S., 2000. Critical periods of vulnerability for the developing nervous system: evidence from humans and animal models. *Environ. Health Perspect.* 108, 511–533. <https://doi.org/10.1289/ehp.00108s3511>.
- Smith, S.M., 2002. Fast robust automated brain extraction. *Hum. Brain Mapp.* 17, 143–155. <https://doi.org/10.1002/hbm.10062>.
- Smith, S.M., Jenkinson, M., Woolrich, M.W., Beckmann, C.F., Behrens, T.E.J., Johansen-Berg, H., Bannister, P.R., De Luca, M., Drobnjak, I., Flitney, D.E., Niazay, R.K., Saunders, J., Vickers, J., Zhang, Y., De Stefano, N., Brady, J.M., Matthews, P.M., 2004. Advances in functional and structural MR image analysis and implementation as FSL. *Neuroimage* 23, 208–219. <https://doi.org/10.1016/j.neuroimage.2004.07.051>.
- Song, S.-K., Sun, S.-W., Ramsbottom, M.J., Chang, C., Russell, J., Cross, A.H., 2002. Demyelination revealed through MRI as increased radial (but unchanged axial) diffusion of water. *Neuroimage* 17, 1429–1436. <https://doi.org/10.1006/nimg.2002.1267>.
- Sowell, E.R., Peterson, B.S., Thompson, P.M., Welcome, S.E., Henkenius, A.L., Toga, A.W., 2003. Mapping cortical change across the human life span. *Nat. Neurosci.* 6, 309–315. <https://doi.org/10.1038/nn1008>.
- Stanisz, G.J., Szafer, A., Wright, G.A., Henkelman, R.M., 1997. An analytical model of restricted diffusion in bovine optic-nerve. *Magn. Reson. Med.* 37, 103–111.
- Taki, Y., Thyreau, B., Hashizume, H., Sassa, Y., Takeuchi, H., Wu, K., Kotozaki, Y., Nouchi, R., Asano, M., Asano, K., Fukuda, H., Kawashima, R., 2013. Linear and curvilinear correlations of brain white matter volume, fractional anisotropy, and mean diffusivity with age using voxel-based and region-of-interest analyses in 246 healthy children. *Hum. Brain Mapp.* 34, 1842–1856. <https://doi.org/10.1002/hbm.22027>.
- Tamnes, C.K., Ostby, Y., Fjell, A.M., Westlye, L.T., Due-Tønnessen, P., Walhovd, K.B., 2010. Brain maturation in adolescence and young adulthood: regional age-related changes in cortical thickness and white matter volume and microstructure. *Cerebr. Cortex* 20, 534–548. <https://doi.org/10.1093/cercor/bhp118>.
- Tau, G.Z., Peterson, B.S., 2010. Normal development of brain circuits. *Neuropsychopharmacology* 35, 147–168. <https://doi.org/10.1038/npp.2009.115>.
- Ullman, H., Klingberg, T., 2016. Timing of white matter development determines cognitive abilities at school entry but not in late adolescence. *Cerebr. Cortex* 1–7. <https://doi.org/10.1093/cercor/bhw256>.
- Ullman, H., Almeida, R., Klingberg, T., 2014. Structural maturation and brain activity predict future working memory capacity during childhood development. *J. Neurosci.* 34, 1592–1598. <https://doi.org/10.1523/JNEUROSCI.0842-13.2014>.
- Vannest, J., Rajagopal, A., Cicchino, N.D., Franks-Henry, J., Simpson, S.M., Lee, G., Altaye, M., Sroka, C., Holland, S.K., Consortium, C.A., 2014. Factors determining success of awake and asleep magnetic resonance imaging scans in nonsedated children. *Neuropediatrics* 45, 370–377.
- Varentsova, A., Zhang, S., Arfanakis, K., 2014. NeuroImage Development of a high angular resolution diffusion imaging human brain template. *Neuroimage* 91, 177–186. <https://doi.org/10.1016/j.neuroimage.2014.01.009>.
- Veraart, J., Sijbers, J., Sunaert, S., Leemans, A., Jeurissen, B., 2013. Weighted linear least squares estimation of diffusion MRI parameters: strengths, limitations, and pitfalls. *Neuroimage* 81, 335–346. <https://doi.org/10.1016/j.neuroimage.2013.05.028>.
- Wakana, S., Caprihan, A., Panzenboeck, M.M., Fallon, J.H., Perry, M., Gollub, R.L., Hua, K., Zhang, J., Jiang, H., Dubey, P., Blitz, A., van Zijl, P., Mori, S., 2007. Reproducibility of quantitative tractography methods applied to cerebral white matter. *Neuroimage* 36, 630–644. <https://doi.org/10.1016/j.neuroimage.2007.02.049>.
- Westlye, L.T., Walhovd, K.B., Dale, A.M., Bjørnerud, A., Due-Tønnessen, P., Engvig, A., Tamnes, C.K., Østby, Y., Fjell, A.M., 2010. Life-span changes of the human brain white matter: diffusion tensor imaging (DTI) and volumetry. *Cerebr. Cortex* 20, 2055–2068. <https://doi.org/10.1093/cercor/bhp280>.
- Wheeler-Kingshott, C.A.M., Cercignani, M., 2009. About “axial” and “radial” diffusivities. *Magn. Reson. Med.* 61, 1255–1260. <https://doi.org/10.1002/mrm.21965>.
- Wierenga, L.M., van den Heuvel, M.P., van Dijk, S., Rijks, Y., de Reus, M.A., Durston, S., 2015. The development of brain network architecture. *Hum. Brain Mapp.* 37, 717–729. <https://doi.org/10.1002/hbm.23062>.
- Woods, R.P., Grafton, S.T., Holmes, C.J., Cherry, S.R., Mazziotta, J.C., 1998. Automated image registration: I. General methods and intrasubject, intramodality validation. *J. Comput. Assist. Tomogr.* 22, 139–152.
- Wu, M., Lu, L.H., Lowe, A., Yang, S., Passarotti, A.M., Zhou, X.J., Pavuluri, M.N., 2014. Development of superficial white matter and its structural interplay with cortical gray matter in children and adolescents. *Hum. Brain Mapp.* 35, 2806–2816. <https://doi.org/10.1002/hbm.22368>.
- Wu, M., Kumar, A., Yang, S., 2016. Development and aging of superficial white matter myelin from young adulthood to old age: mapping by vertex-based surface statistics (VBSS). *Hum. Brain Mapp.* 37, 1759–1769. <https://doi.org/10.1002/hbm.23134>.
- Yakovlev, P., Lecours, A., 1967. The myelogenetic cycles of regional maturation of the brain. In: *Regional Development of the Brain in Early Life*. Blackwell, Oxford.
- Yeatman, J.D., Dougherty, R.F., Ben-Shachar, M., Wandell, B.A., 2012a. Development of white matter and reading skills. *Proc. Natl. Acad. Sci. Unit. States Am.* 109, E3045–E3053. <https://doi.org/10.1073/pnas.1206792109>.
- Yeatman, Jason D., Dougherty, R.F., Myall, N.J., Wandell, B.A., Feldman, H.M., 2012b. Tract profiles of white matter properties: automating fiber-tract quantification. *PLoS One* 7. <https://doi.org/10.1371/journal.pone.0049790>.
- Yuan, W., Altaye, M., Ret, J., Schmithorst, V., Byars, A.W., Plante, E., Holland, S.K., 2009. Quantification of head motion in children during various fMRI language tasks. *Hum. Brain Mapp.* 30, 1481–1489. <https://doi.org/10.1002/hbm.20616>.
- Zhang, H., Yushkevich, P.A., Alexander, D.C., Gee, J.C., 2006. Deformable registration of diffusion tensor MR images with explicit orientation optimization. *Med. Image Anal.* 10, 764–785. <https://doi.org/10.1016/j.media.2006.06.004>.
- Zhang, H., Hubbard, P.L., Parker, G.J.M., Alexander, D.C., 2011a. Axon diameter mapping in the presence of orientation dispersion with diffusion MRI. *Neuroimage* 56, 1301–1315. <https://doi.org/10.1016/j.neuroimage.2011.01.084>.
- Zhang, S., Peng, H., Dawe, R.J., Arfanakis, K., 2011b. NeuroImage Enhanced ICBM diffusion tensor template of the human brain. *Neuroimage* 54, 974–984. <https://doi.org/10.1016/j.neuroimage.2010.09.008>.
- Zhang, H., Schneider, T., Wheeler-Kingshott, C.A., Alexander, D.C., 2012. NODDI: practical in vivo neurite orientation dispersion and density imaging of the human brain. *Neuroimage* 61, 1000–1016. <https://doi.org/10.1016/j.neuroimage.2012.03.072>.